

## Measurement of the Target-Normal Single-Spin Asymmetry in Deep-Inelastic Scattering from the Reaction ${}^3\text{He}^\uparrow(e,e')X$

J. Katich,<sup>1,2</sup> X. Qian,<sup>3,4,5</sup> Y. X. Zhao,<sup>6</sup> K. Allada,<sup>7</sup> K. Aniol,<sup>8</sup> J. R. M. Annand,<sup>9</sup> T. Averett,<sup>1,†</sup> F. Benmokhtar,<sup>10</sup> W. Bertozzi,<sup>11</sup> P. C. Bradshaw,<sup>1</sup> P. Bosted,<sup>1</sup> A. Camsonne,<sup>12</sup> M. Canan,<sup>13</sup> G. D. Cates,<sup>14</sup> C. Chen,<sup>15</sup> J.-P. Chen,<sup>12</sup> W. Chen,<sup>3</sup> K. Chirapatpimol,<sup>14</sup> E. Chudakov,<sup>12</sup> E. Cisbani,<sup>16,17</sup> J. C. Cornejo,<sup>8</sup> F. Cusanno,<sup>16,17</sup> M. M. Dalton,<sup>14</sup> W. Deconinck,<sup>11</sup> C. W. de Jager,<sup>12,14</sup> R. De Leo,<sup>18</sup> X. Deng,<sup>14</sup> A. Deur,<sup>12</sup> H. Ding,<sup>14</sup> P. A. M. Dolph,<sup>14</sup> C. Dutta,<sup>7</sup> D. Dutta,<sup>19</sup> L. El Fassi,<sup>13,20</sup> S. Frullani,<sup>16,17</sup> H. Gao,<sup>3</sup> F. Garibaldi,<sup>16,17</sup> D. Gaskell,<sup>12</sup> S. Gilad,<sup>11</sup> R. Gilman,<sup>12,20</sup> O. Glamazdin,<sup>21</sup> S. Golge,<sup>13</sup> L. Guo,<sup>22</sup> D. Hamilton,<sup>9</sup> O. Hansen,<sup>12</sup> D. W. Higinbotham,<sup>12</sup> T. Holmstrom,<sup>23</sup> J. Huang,<sup>11</sup> M. Huang,<sup>3</sup> H. F. Ibrahim,<sup>24</sup> M. Iodice,<sup>25</sup> X. Jiang,<sup>20,22</sup> G. Jin,<sup>14</sup> M. K. Jones,<sup>12</sup> A. Kelleher,<sup>1</sup> W. Kim,<sup>26</sup> A. Kolarkar,<sup>7</sup> W. Korsch,<sup>7</sup> J. J. LeRose,<sup>12</sup> X. Li,<sup>27</sup> Y. Li,<sup>27</sup> R. Lindgren,<sup>14</sup> N. Liyanage,<sup>14</sup> E. Long,<sup>28</sup> H.-J. Lu,<sup>6</sup> D. J. Margaziotis,<sup>8</sup> P. Markowitz,<sup>29</sup> S. Marrone,<sup>18</sup> D. McNulty,<sup>30</sup> Z.-E. Meziani,<sup>31</sup> R. Michaels,<sup>12</sup> B. Moffit,<sup>11,12</sup> C. Muñoz Camacho,<sup>32</sup> S. Nanda,<sup>12</sup> A. Narayan,<sup>19</sup> V. Nelyubin,<sup>14</sup> B. Norum,<sup>14</sup> Y. Oh,<sup>33</sup> M. Osipenko,<sup>34</sup> D. Parno,<sup>10</sup> J. C. Peng,<sup>35</sup> S. K. Phillips,<sup>28</sup> M. Posik,<sup>31</sup> A. J. R. Puckett,<sup>11,22</sup> Y. Qiang,<sup>3,12</sup> A. Rakhman,<sup>36</sup> R. D. Ransome,<sup>20</sup> S. Riordan,<sup>14</sup> A. Saha,<sup>12,\*</sup> B. Sawatzky,<sup>12,31</sup> E. Schulte,<sup>20</sup> A. Shahinyan,<sup>37</sup> M. H. Shabestari,<sup>14</sup> S. Širca,<sup>38</sup> S. Stepanyan,<sup>39</sup> R. Subedi,<sup>14</sup> V. Sulkosky,<sup>11,12</sup> L.-G. Tang,<sup>15</sup> A. Tobias,<sup>14</sup> G. M. Urciuoli,<sup>16</sup> I. Vilardi,<sup>18</sup> K. Wang,<sup>14</sup> Y. Wang,<sup>35</sup> B. Wojtsekhowski,<sup>12</sup> X. Yan,<sup>6</sup> H. Yao,<sup>31</sup> Y. Ye,<sup>6</sup> Z. Ye,<sup>15</sup> L. Yuan,<sup>15</sup> X. Zhan,<sup>11</sup> Y. Zhang,<sup>40</sup> Y.-W. Zhang,<sup>40</sup> B. Zhao,<sup>1</sup> X. Zheng,<sup>14</sup>

L. Zhu,<sup>15,35</sup> X. Zhu,<sup>3</sup> and X. Zong<sup>3</sup>

<sup>1</sup>College of William and Mary, Williamsburg, Virginia 23187, USA

<sup>2</sup>University of Colorado, Boulder, Colorado 80309, USA

<sup>3</sup>Duke University, Durham, North Carolina 27708, USA

<sup>4</sup>Kellogg Radiation Laboratory, California Institute of Technology, Pasadena, California 91125, USA

<sup>5</sup>Brookhaven National Laboratory, Upton, New York 11973, USA

<sup>6</sup>University of Science and Technology of China, Hefei 230026, People's Republic of China

<sup>7</sup>University of Kentucky, Lexington, Kentucky 40506, USA

<sup>8</sup>California State University, Los Angeles, Los Angeles, California 90032, USA

<sup>9</sup>University of Glasgow, Glasgow G12 8QQ, Scotland, United Kingdom

<sup>10</sup>Carnegie Mellon University, Pittsburgh, Pennsylvania 15213, USA

<sup>11</sup>Massachusetts Institute of Technology, Cambridge, Massachusetts 02139, USA

<sup>12</sup>Thomas Jefferson National Accelerator Facility, Newport News, Virginia 23606, USA

<sup>13</sup>Old Dominion University, Norfolk, Virginia 23529, USA

<sup>14</sup>University of Virginia, Charlottesville, Virginia 22904, USA

<sup>15</sup>Hampton University, Hampton, Virginia 23187, USA

<sup>16</sup>INFN, Sezione di Roma, I-00161 Rome, Italy

<sup>17</sup>Istituto Superiore di Sanità, I-00161 Rome, Italy

<sup>18</sup>INFN, Sezione di Bari and University of Bari, I-70126 Bari, Italy

<sup>19</sup>Mississippi State University, Mississippi State, Minnesota 39762, USA

<sup>20</sup>Rutgers, The State University of New Jersey, Piscataway, New Jersey 08855, USA

<sup>21</sup>Kharkov Institute of Physics and Technology, Kharkov 61108, Ukraine

<sup>22</sup>Los Alamos National Laboratory, Los Alamos, New Mexico 87545, USA

<sup>23</sup>Longwood University, Farmville, Virginia 23909, USA

<sup>24</sup>Cairo University, Giza 12613, Egypt

<sup>25</sup>INFN, Sezione di Roma3, I-00146 Rome, Italy

<sup>26</sup>Kyungpook National University, Taegu 702-701, Republic of Korea

<sup>27</sup>China Institute of Atomic Energy, Beijing, People's Republic of China

<sup>28</sup>University of New Hampshire, Durham, New Hampshire 03824, USA

<sup>29</sup>Florida International University, Miami, Florida 33199, USA

<sup>30</sup>University of Massachusetts, Amherst, Massachusetts 01003, USA

<sup>31</sup>Temple University, Philadelphia, Pennsylvania 19122, USA

<sup>32</sup>Université Blaise Pascal/IN2P3, F-63177 Aubière, France

<sup>33</sup>Seoul National University, Seoul, 151-747, Republic of Korea

<sup>34</sup>INFN, Sezione di Genova, I-16146 Genova, Italy

<sup>35</sup>University of Illinois at Urbana-Champaign, Urbana, Illinois 61801, USA

<sup>36</sup>Syracuse University, Syracuse, New York 13244, USA

<sup>37</sup>Yerevan Physics Institute, Yerevan 375036, Armenia

<sup>38</sup>University of Ljubljana, SI-1000 Ljubljana, Slovenia

<sup>39</sup>Kyungpook National University, Daegu 702-701, Republic of Korea<sup>40</sup>Lanzhou University, Lanzhou 730000, Gansu, People's Republic of China

(Received 7 November 2013; revised manuscript received 13 March 2014; published 11 July 2014)

We report the first measurement of the target-normal single-spin asymmetry in deep-inelastic scattering from the inclusive reaction  ${}^3\text{He}^\uparrow(e, e')X$  on a polarized  ${}^3\text{He}$  gas target. Assuming time-reversal invariance, this asymmetry is strictly zero in the Born approximation but can be nonzero if two-photon-exchange contributions are included. The experiment, conducted at Jefferson Lab using a 5.89 GeV electron beam, covers a range of  $1.7 < W < 2.9$  GeV,  $1.0 < Q^2 < 4.0$  GeV<sup>2</sup> and  $0.16 < x < 0.65$ . Neutron asymmetries were extracted using the effective nucleon polarization and measured proton-to- ${}^3\text{He}$  cross-section ratios. The measured neutron asymmetries are negative with an average value of  $(-1.09 \pm 0.38) \times 10^{-2}$  for invariant mass  $W > 2$  GeV, which is nonzero at the  $2.89\sigma$  level. Our measured asymmetry agrees both in sign and magnitude with a two-photon-exchange model prediction that uses input from the Sivers transverse momentum distribution obtained from semi-inclusive deep-inelastic scattering.

DOI: 10.1103/PhysRevLett.113.022502

PACS numbers: 25.30.Dh, 14.20.Dh, 24.70.+s, 29.25.Pj

The past decade has seen a resurrection of interest in two-photon exchange in electron-nucleon scattering. This is primarily due to the realization that inclusion of the two-photon-exchange amplitude can partially reconcile the discrepancy between the Rosenbluth separation and the polarization-transfer methods for extracting the  $Q^2$  dependence of the proton elastic form factor ratio,  $G_E^p/G_M^p$  [1–8]. As the precision of nucleon structure measurements improves, it is important to understand the dynamics of the two-photon-exchange processes. Assuming conservation of parity and time-reversal invariance, the target single-spin asymmetry (SSA) in  $(e, e')$  from a target polarized normal to the electron scattering plane is strictly zero at Born level [9], but can be nonzero when interference between one- and two-photon exchange processes is included (Fig. 1).

Consider the inelastic scattering of an unpolarized electron from a target nucleon with vector spin  $\vec{S}$ , oriented perpendicular (transversely polarized) to the incident electron three-momentum  $\vec{k}$ , with normalization  $|\vec{S}| = 1$ . Requiring conservation of the electromagnetic current and parity, the differential cross section,  $d\sigma$ , for inclusive scattering is written as [9–11]

$$\begin{aligned} d\sigma(\phi_S) &= d\sigma_{UU} + \frac{\vec{S} \cdot (\vec{k} \times \vec{k}')}{|\vec{k} \times \vec{k}'|} d\sigma_{UT} \\ &= d\sigma_{UU} + d\sigma_{UT} \sin \phi_S, \end{aligned} \quad (1)$$

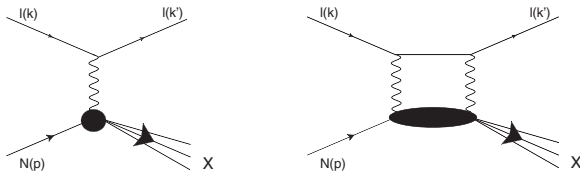


FIG. 1. Interference between one- and two-photon exchange in  $N(e, e')$  allows the possibility of a nonzero target SSA. Here,  $l$  is the lepton with incident and outgoing four-momenta  $k$  and  $k'$ , respectively.  $N$  is the nucleon with initial four-momentum  $p$ .

where  $\vec{k}'$  is the three-momentum of the scattered electron, and  $d\sigma_{UU}$  and  $d\sigma_{UT}$  are the cross sections for an unpolarized electron scattered from an unpolarized and transversely polarized target, respectively. Our choice of coordinates is shown in Fig. 2 with the angle  $\phi_S$  between the lepton plane and  $\vec{S}$ . The  $+\hat{y}$  direction is parallel to the vector  $\vec{k} \times \vec{k}'$  and corresponds to  $\phi_S = 90^\circ$ . We define the SSA as

$$A_{UT}(\phi_S) = \frac{d\sigma(\phi_S) - d\sigma(\phi_S + \pi)}{d\sigma(\phi_S) + d\sigma(\phi_S + \pi)} = A_y \sin \phi_S. \quad (2)$$

The quantity  $A_y \equiv d\sigma_{UT}/d\sigma_{UU}$  can be extracted by measuring the  $\phi_S$  dependence of  $A_{UT}(\phi_S)$ , or by measuring the SSA for a target polarized normal to the lepton plane.

Considering only the one-photon-exchange amplitude,  $\mathcal{M}_{1\gamma}$ , we can write  $d\sigma_{UU} \propto \text{Re}(\mathcal{M}_{1\gamma}\mathcal{M}_{1\gamma}^*)$  and  $d\sigma_{UT} \propto \text{Im}(\mathcal{M}_{1\gamma}\mathcal{M}_{1\gamma}^*)$ , where  $\text{Re}$  ( $\text{Im}$ ) stands for the real (imaginary) part. However time-reversal invariance requires that  $\mathcal{M}_{1\gamma}$  be real and so at order  $\alpha_{em}^2$ ,  $d\sigma_{UU}$  can be nonzero but  $d\sigma_{UT}$  must be zero. When one includes the (complex) two-photon-exchange amplitude,  $\mathcal{M}_{2\gamma}$ , the contribution to the asymmetry from one- and two-photon interference is  $d\sigma_{UT} \propto \text{Im}(\mathcal{M}_{1\gamma}\mathcal{M}_{2\gamma}^*)$  which can be nonzero at order

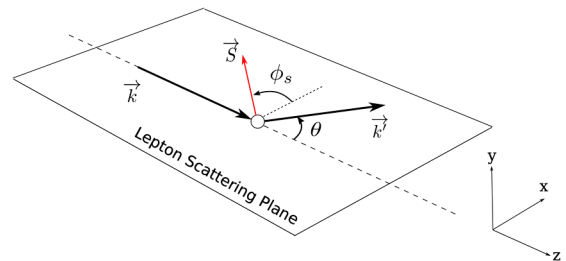


FIG. 2 (color online). Coordinate system used to define  $A_{UT}(\phi_S)$ .

$\alpha_{em}^3$ . The two-photon exchange process forms a loop with the nucleon intermediate state and contains the full response of the nucleon (see Fig. 1).

An additional contribution to  $d\sigma_{UT}$  at order  $\alpha_{em}^3$  may arise from interference between real photon emission (bremsstrahlung) by the electron and the hadronic system. Detailed discussions of these contributions are presented in Refs. [11–13].

There are no published measurements of  $A_y$  for the neutron. For protons, the first measurement of  $A_y^p$  was done in 1968 at CEA [14]. Electrons were scattered from an alcohol/water target containing protons with an average polarization  $\sim 20\%$ . Three invariant photon-hadron masses were studied,  $W = 1236, 1512,$  and  $1688$  MeV, with  $Q^2 = 0.2\text{--}0.7$  GeV<sup>2</sup>. Results were consistent with zero at the  $4 \times 10^{-2}$  level. In 1969 a measurement at SLAC [15] was made using both  $e^-$  and  $e^+$  scattering in the resonance region with  $Q^2 = 0.4\text{--}1.0$  GeV<sup>2</sup>. A butanol target provided protons with a polarization of  $\sim 20\%$ . Results were consistent with zero at the few  $\times 10^{-2}$  level.

A theoretical calculation for  $A_y^p$  at  $W = 1232$  MeV [10] treated the intermediate state as purely elastic and predicted  $A_y^p \sim 0.75 \times 10^{-2}$  at  $Q^2 = 0.6$  GeV<sup>2</sup>.

The only measurement of  $A_y^p$  using deep-inelastic scattering (DIS) was made at DESY by the HERMES collaboration [16]. Both  $e^-$  and  $e^+$  with energy 27.6 GeV were scattered from a polarized hydrogen target with average polarization  $\sim 75\%$ . Particles were detected over  $0.007 < x_B < 0.9, 0.25 < Q^2 < 20$  GeV<sup>2</sup> and  $\phi_S = 0\text{--}2\pi$ . Results for  $A_y^p$  for  $Q^2 > 1$  GeV<sup>2</sup> are consistent with zero at the  $\sim 10^{-3}$  level.

There are two parton-model predictions for the two-photon exchange contribution to  $A_y$  for protons and neutrons in DIS. The first, by A. Afanasev *et al.* [11], assumes the scattering is dominated by two-photon exchange with a single quark and predicts  $A_y^n \sim 10^{-4}$  at  $x \sim 0.3$  and  $Q^2 = 2.0$  GeV<sup>2</sup>. In the second prediction, A. Metz *et al.* [12] assume the asymmetry is dominated by the process where one of the photons couples to an active quark and the other couples to a quark in the spectator di-quark system. When the interaction with the di-quark system is modeled using input from the Sivers distributions from semi-inclusive DIS [17,18], they predict  $A_y^n \sim -10^{-2}$  at the kinematics of our experiment. For consistency with our sign convention, the asymmetries in Ref. [12] have been multiplied by  $-1$ .

This paper presents the results of Jefferson Lab experiment E07-013, which was a measurement of the neutron SSA,  $A_y^n$ , in DIS. The  $\phi_S$ -dependent asymmetries were measured using inclusive scattering of unpolarized electrons from a <sup>3</sup>He target polarized either vertically ( $\phi_S \sim \pm 90^\circ$ ) or transversely ( $\phi_S \sim 0^\circ, 180^\circ$ ) in the lab frame.  $A_y$  was obtained by fitting the  $\phi_S$  dependence according to Eq. (2). The nuclear ground state of <sup>3</sup>He is dominated by the configuration in which the spins of two protons are anti-aligned,

which means that the spin is mostly carried by the neutron, effectively providing a polarized neutron target.

An electron beam with energy 5.889 GeV and average current 12  $\mu$ A was incident on polarized <sup>3</sup>He gas with density  $\sim 10$  amg contained in a 40-cm-long cylindrical aluminosilicate glass cell. The beam was rastered in a  $3 \times 3$  mm<sup>2</sup> pattern to reduce the possibility of cell rupture and localized depolarization. Polarization of the <sup>3</sup>He nuclei was achieved via spin-exchange optical pumping (SEOP) with a hybrid alkali-metal mixture of Rb and K [19]. The polarization direction was reversed every 20 minutes using adiabatic fast passage nuclear magnetic resonance (NMR). With each spin-flip, the NMR signals were used to measure the relative polarization. Absolute calibration was done periodically throughout the run using electron paramagnetic resonance [20]. The average polarization was 55% with a 5% relative uncertainty. The total luminosity downstream of the target was measured during each 20-minute target polarization state using eight Lucite/PMT detectors placed symmetrically around the beam line. The average luminosity asymmetry for the experiment was  $(38 \pm 12) \times 10^{-6}$  which is negligible compared to our measured raw asymmetries of  $\sim 10^{-3}$ .

Scattered electrons were detected using the Hall A BigBite detector package [21] at  $+30^\circ$  (beam-right) and the left Hall A high resolution spectrometer (LHRS) at  $-16^\circ$  [22]. The BigBite package includes a dipole magnet for momentum separation, three sets of multiwire drift chambers for track reconstruction, and a lead-glass electromagnetic calorimeter for particle identification (PID) with preshower and shower layers sandwiching a scintillator plane for providing timing information. The useful momentum coverage of BigBite was  $0.6 < p < 2.5$  GeV with an average solid angle acceptance of 64 msr. The corresponding  $\phi_S$  coverage is  $\sim 60^\circ$  for each target polarization configuration. The LHRS consists of two sets of drift chambers for tracking, two scintillator planes for the trigger, and gas Cherenkov and lead-glass shower detectors for PID. The central momentum of the LHRS was 2.35 GeV with a momentum coverage of  $\pm 4.5\%$ . The solid angle acceptance was  $\sim 6$  msr with  $\sim 7^\circ$   $\phi_S$  coverage. Optics for both detectors were calibrated using elastic  $e^-$  scattering from hydrogen and multi-foil carbon targets. Angular reconstruction in both detectors was calibrated using a sieve slit placed in front of each spectrometer. The angular resolution in BigBite was  $< 10$  mrad and the resolution of the reconstructed momentum was  $< 1\%$ .

Electron PID in BigBite began at the trigger level, which required the sum of the preshower and shower signals to be above a chosen threshold. Events with poor track reconstruction, tracks near the edges of the acceptance, and data that could be affected by beam trips were removed. Additional cuts included particle charge, reconstructed particle momentum, reconstructed vertex, energy deposited in the preshower detector ( $E_{ps} > 200$  MeV), and a cut on

the ratio of reconstructed energy to reconstructed momentum ( $E/p$ ). The LHRS cuts were similar and included cuts on the reconstructed vertex, Cherenkov amplitude, and an  $E/p$  cut. The data from BigBite covered  $0.17 < x < 0.65$  and were divided into five bins in  $W$ . The LHRS data were analyzed as a single kinematic point ( $x = 0.16$ ,  $W = 2.54$  GeV).

Events from three triggers taken simultaneously were used in the BigBite analysis. They are T1, proportional to the total energy deposited in the calorimeter, T6, which is the same as T1 but with higher discriminator threshold, and T2, coincidence between a gas Cherenkov detector and T6. Prescale factors ranging from 2100 to 3100, 61 to 410, and 350 to 780 were used for T1, T2, and T6, respectively. Because the background rate from the Cherenkov detector was extremely high, the T2 trigger is functionally the same as the T6 trigger. Information from the Cherenkov detector was not used in this analysis. In the final data set, T6 contributes to more than 80% of the data, while T2 is about 12%, and T1 is less than 8%.

Raw asymmetries for each data bin were formed as

$$A_{\text{raw}}^{e^-}(\phi_S) = \frac{1}{P_{\text{target}}} \frac{Y_{\text{raw}}^{\uparrow}(\phi_S) - Y_{\text{raw}}^{\downarrow}(\phi_S + \pi)}{Y_{\text{raw}}^{\uparrow}(\phi_S) + Y_{\text{raw}}^{\downarrow}(\phi_S + \pi)}, \quad (3)$$

where the raw yields,  $Y_{\text{raw}}^{\uparrow(\downarrow)}$ , are the number of particles,  $N$ , observed in the target spin “up” (“down”) state that pass all data cuts for electrons, normalized by accumulated charge,  $Q$ , and DAQ live time,  $LT$ :

$$Y_{\text{raw}}^{\uparrow(\downarrow)} = \frac{N_{\text{raw}}^{\uparrow(\downarrow)}}{Q^{\uparrow(\downarrow)}LT^{\uparrow(\downarrow)}} = \frac{N_{e^-}^{\uparrow(\downarrow)} + N_{\pi^-}^{\uparrow(\downarrow)} + N_{e^+}^{\uparrow(\downarrow)}}{Q^{\uparrow(\downarrow)}LT^{\uparrow(\downarrow)}}. \quad (4)$$

The terms  $N_{\pi^-}$  and  $N_{e^+}$  represent pion and pair-produced electron backgrounds that pass the good-electron cuts and  $P_{\text{target}}$  is the target polarization. The  $\phi_S$  angle is defined for the spin up state, and changed by  $180^\circ$  ( $\phi_S + \pi$ ) when the target spin was flipped.

The dominant background passing the data cuts in BigBite were photoinduced electron-positron pairs. The positrons were cut from the data by requiring particles with

negative charge. However, the pair-produced electrons are indistinguishable from the desired DIS electrons. A direct measurement of the pair-produced electron contamination was made by reversing the polarity of the BigBite magnet and calculating the positron yield under conditions identical to the normal data collection. Since photons are mostly produced from neutral pion decay, the contamination decreased with increasing momentum, see Table I. This also explains why this type of background in the LHRS (central momentum of 2.35 GeV) is negligible. Negative pions were also a source of contamination. Their contributions to the BigBite data were accounted for by fitting the preshower energy spectrum. Likewise, the positron data sample was contaminated by positive pions. The positive pion contamination was estimated based on the negative pion contamination. A GEANT-based Monte Carlo simulation of the BigBite spectrometer was used to study the differences between the  $\pi^+$  and  $\pi^-$  contaminations. Data from the LHRS were relatively free of background contamination due to the choice of kinematics and exceptional PID.

Due to the large acceptance of the BigBite spectrometer, asymmetries for each type of background particle ( $A^{\pi^-}$ ,  $A_{\text{raw}}^{e^+}$ , and  $A^{\pi^+}$ ) were obtained from the data in the same way as  $A_{\text{raw}}^{e^-}$  but with different selection cuts: (i) positrons were selected using the same cuts as electrons except for the particle charge and (ii) pions were selected using the same cuts as electrons or positrons except for requiring a preshower energy deposition under 150 MeV. Corrections were made to the asymmetry via

$$A^{e^-} = \frac{A_{\text{raw}}^{e^-} - f_1 A^{\pi^-} - f_4(1 - f_3) \frac{A_{\text{raw}}^{e^+} - f_5 A^{\pi^+}}{1 - f_5}}{1 - f_1 - f_4(1 - f_3)}, \quad (5)$$

where the coefficients,  $f_i$ , give the fractions of misidentified particles and are defined as

$$\begin{aligned} f_1 &= Y_{\text{neg}}^{\pi^-} / (Y_{\text{neg}}^{e^-} + Y_{\text{neg}}^{\pi^-}) \\ f_3 &= Y_{\text{pos}}^{\pi^+} / (Y_{\text{pos}}^{e^+} + Y_{\text{pos}}^{\pi^+}) \\ f_4 &= (Y_{\text{pos}}^{e^+} + Y_{\text{pos}}^{\pi^+}) / (Y_{\text{neg}}^{e^-} + Y_{\text{neg}}^{\pi^-}) \\ f_5 &= Y_{\text{neg}}^{\pi^+} / (Y_{\text{neg}}^{e^+} + Y_{\text{neg}}^{\pi^+}). \end{aligned} \quad (6)$$

TABLE I. Kinematics and results for neutron asymmetries with statistical and systematic uncertainties. The BigBite spectrometer was set at a fixed angle and central momentum and data were divided into the five kinematic bins. The final column shows measured contaminations from pair-produced electrons.

Detector	$W$ GeV	$x$	$Q^2$ GeV <sup>2</sup>	$A_y^{3\text{He}} \pm (\text{stat}) \pm (\text{syst}) (\times 10^{-3})$	$A_y^n \pm (\text{stat}) \pm (\text{syst}) (\times 10^{-2})$	Pair-produced background contamination (%)
BigBite	1.72	0.65	3.98	$-0.85 \pm 2.79 \pm 0.53$	$-0.55 \pm 1.81 \pm 0.36$	$1.0 \pm 0.8$
BigBite	2.17	0.46	3.24	$-6.28 \pm 2.51 \pm 0.88$	$-3.87 \pm 1.55 \pm 0.58$	$3.1 \pm 1.1$
BigBite	2.46	0.34	2.65	$-8.14 \pm 1.99 \pm 1.05$	$-3.89 \pm 0.96 \pm 0.53$	$9.5 \pm 2.0$
BigBite	2.70	0.24	2.08	$-2.25 \pm 2.45 \pm 1.46$	$-1.08 \pm 1.18 \pm 0.69$	$22.0 \pm 4.5$
BigBite	2.89	0.17	1.58	$-8.34 \pm 4.35 \pm 5.33$	$-3.84 \pm 2.00 \pm 2.42$	$48 \pm 10$
LHRS	2.54	0.16	1.05	$-1.57 \pm 0.99 \pm 0.2$	$-0.64 \pm 0.41 \pm 0.09$	$1.3 \pm 0.05$



The pos and neg subscripts indicate the polarity of the BigBite magnet (standard running conditions are neg). The  $f_5$  were estimated based on  $f_3$ . Further information on these background corrections is provided as Supplemental Material [23].

A small quantity of unpolarized  $N_2$  was used in the  $^3\text{He}$  target-cell to improve the efficiency of the optical pumping. The asymmetry was corrected by a dilution factor defined as

$$\eta_{N_2} \equiv \frac{1}{1 + \left(\frac{\rho_{N_2}}{\rho_{^3\text{He}}}\right) \left(\frac{\sigma_{N_2}}{\sigma_{^3\text{He}}}\right)}, \quad (7)$$

where  $\rho$  are the densities and  $\sigma$  are the unpolarized cross sections for each gas. The ratio of densities is taken from the target cell filling data. The cross-section ratio is determined experimentally by inelastic scattering from a reference cell filled with known densities of either  $N_2$  or  $^3\text{He}$ . The dilution factors for BigBite measured for T1 and T6 triggers agree with each other. The final dilution was determined by combining results from T1 and T6 according to their statistical uncertainties, giving  $\eta \sim 0.9$  for all kinematics with an uncertainty of  $\sim 2\%$ . The dilution factor for the LHRS was determined to be  $0.851 \pm 0.018$ . The  $^3\text{He}$  asymmetries from BigBite T1, T2 and T6 triggers were extracted independently and were consistent with each other within the statistical uncertainties for each bin. The final  $^3\text{He}$  asymmetries were obtained by combining the results from the T1, T2 and T6 asymmetries according to their statistical uncertainties.

Neutron asymmetries were obtained from the  $^3\text{He}$  asymmetries using the effective polarizations of the proton and neutron in polarized  $^3\text{He}$  using [24],

$$A_y^{^3\text{He}} = (1 - f_p)P_n A_y^n + f_p P_p A_y^p. \quad (8)$$

Here,  $P_n = 0.86^{+0.036}_{-0.02}$  ( $P_p = -0.028^{+0.009}_{-0.004}$ ) is the effective neutron (proton) polarization [25].

The proton dilutions of  $^3\text{He}$  for BigBite,  $f_p = 2\sigma_p/\sigma_{^3\text{He}}$ , were measured for the T1 and T6 triggers using the yields from unpolarized hydrogen and  $^3\text{He}$  targets and are consistent with each other. The final dilutions, which varied between 0.75–0.82, with uncertainties of 0.02–0.08, were determined by combining the T1 and T6 results according to their statistical uncertainties. Neutron asymmetries were calculated separately for each trigger type and combined according to their statistical uncertainties. The proton dilution for the LHRS was  $0.715 \pm 0.007$ . A value of  $A_y^p = (0 \pm 3) \times 10^{-3}$  was used in Eqn. (8) based on the HERMES measurements [16]. External radiative corrections were applied to both the BigBite and LHRS data using a Monte Carlo simulation that included detailed modeling of geometry and material in the target and spectrometers. No correction was made on the asymmetries since the radiative corrections to the two-photon exchange process are not yet available and the phase space of this measurement is limited.

The dominant systematic uncertainty for BigBite is from background contamination, the largest of which is from pair-produced electrons (see Table I). The  $\pi^-$  contamination in the T6 triggers ranges from 0.5% to 2.0% (rel.) from the lowest to highest  $W$  bin, respectively. The uncertainties on the contamination are  $\sim 0.5\%$ , which were estimated using the difference between information from the Monte Carlo simulation and contamination estimation based on data. Further details about these corrections for the other two triggers (T1 and T2) can be found in the Supplemental Material [23]. The uncertainties associated with backgrounds contribute to both the asymmetries and dilution factors. The final results were extracted taking into account the full correlation of these uncertainties. Other BigBite systematic uncertainties include the detector acceptance ( $1.2 \times 10^{-4}$ ), detector response drift ( $9 \times 10^{-5}$ ), and live time asymmetry ( $6 \times 10^{-5}$ ). For the LHRS, systematic uncertainties include the live time asymmetry ( $6 \times 10^{-5}$ ) and tracking efficiency ( $7 \times 10^{-5}$ ). The correction to the LHRS asymmetry due to pair-produced electrons is  $1.56 \times 10^{-4}$  with a 100% relative uncertainty. Systematic uncertainties from the polarized target include target polarization and misalignment (5%), and luminosity fluctuations ( $1.2 \times 10^{-5}$ ).

The  $^3\text{He}$  and neutron results are presented in Table I along with the pair-produced electron contamination. Neutron results are shown in Fig. 3. The asymmetry is generally negative and nonzero across the measured kinematic range. At the largest value of  $W$ , the systematic uncertainty is quite large due to the uncertainty in the pair-produced electron contamination. In order to evaluate how much the data

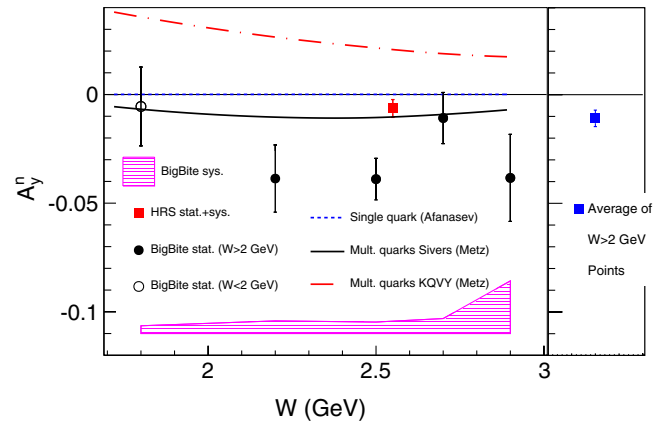


FIG. 3 (color online). Neutron asymmetry results (color online). Left panel: Solid black data points are DIS data ( $W > 2$  GeV) from the BigBite spectrometer; open circle has  $W = 1.72$  GeV. BigBite data points show statistical uncertainties with systematic uncertainties indicated by the lower solid band. The square point is the LHRS data with combined statistical and systematic uncertainties. The dotted curve near zero (positive) is the calculation by A. Afanasev *et al.* [11], The solid and dot-dashed curves are calculations by A. Metz *et al.* [12] (multiplied by  $-1$ ). Right panel: The average measured asymmetry for the DIS data with combined systematic and statistical uncertainties.

disfavors the zero-asymmetry hypothesis in the DIS region, the average asymmetry was calculated for the data with  $W > 2.0$  GeV. Because the systematic uncertainties of the BigBite points are mostly due to background contamination, they were assumed to be fully correlated, and uncorrelated with the LHRS point. The final average neutron asymmetry in the DIS region and its total experimental uncertainty are determined to be  $(-1.09 \pm 0.38) \times 10^{-2}$ , which is nonzero at the  $2.89\sigma$  level. The data are in good agreement with the two-photon exchange prediction by A. Metz *et al.* [12],  $A_y^n \sim -10^{-2}$ , that uses model input from the semi-inclusive DIS Sivvers distribution.

We have presented the first measurements of the neutron target-normal SSA,  $A_y^n$ , in the DIS region using a polarized  $^3\text{He}$  target. Because  $A_y$  must be zero at Born-level its measurement is a valuable laboratory for studying two-photon exchange and the dynamics of the nucleon beyond the simple quark-parton model. Further measurements for both proton and neutron with higher precision over a broader kinematic range are necessary to gain a deeper understanding of the role of two-photon exchange in nucleon structure studies.

We acknowledge the outstanding support of the Jefferson Lab Hall A technical staff and Accelerator Division in accomplishing this experiment. We thank A. Afanasev, C. Weiss, and A. Metz for their valuable theoretical guidance. This work was supported in part by the U.S. National Science Foundation, the UK Science and Technology Facilities Council, the U.S. Department of Energy and by DOE Contract No. DE-AC05-06OR23177, under which Jefferson Science Associates, LLC, operates the Thomas Jefferson National Accelerator Facility.

---

\*Deceased.

†Corresponding author.  
tdaver@wm.edu

[1] J. Arrington, *Phys. Rev. C* **68**, 034325 (2003).

[2] J. Arrington, P. Blunden, and W. Melnitchouk, *Prog. Part. Nucl. Phys.* **66**, 782 (2011).

- [3] M. Christy *et al.* (E94110 Collaboration), *Phys. Rev. C* **70**, 015206 (2004).
- [4] I. Qattan, J. Arrington, R. Segel, X. Zheng, K. Aniol *et al.*, *Phys. Rev. Lett.* **94**, 142301 (2005).
- [5] A. Puckett, E. Brash, O. Gayou, M. Jones, L. Pentchev *et al.*, *Phys. Rev. C* **85**, 045203 (2012).
- [6] P. G. Blunden, W. Melnitchouk, and J. A. Tjon, *Phys. Rev. Lett.* **91**, 142304 (2003).
- [7] Y. C. Chen, A. Afanasev, S. J. Brodsky, C. E. Carlson, and M. Vanderhaeghen, *Phys. Rev. Lett.* **93**, 122301 (2004).
- [8] C. E. Carlson and M. Vanderhaeghen, *Annu. Rev. Nucl. Part. Sci.* **57**, 171 (2007).
- [9] N. Christ and T. D. Lee, *Phys. Rev.* **143**, 1310 (1966).
- [10] R. N. Cahn and Y. S. Tsai, *Phys. Rev. D* **2**, 870 (1970).
- [11] A. Afanasev, M. Strikman, and C. Weiss, *Phys. Rev. D* **77**, 014028 (2008).
- [12] A. Metz, D. Pitonyak, A. Schäfer, M. Schlegel, W. Vogelsang, and J. Zhou, *Phys. Rev. D* **86**, 094039 (2012).
- [13] M. Schlegel, *Phys. Rev. D* **87**, 034006 (2013).
- [14] J. R. Chen *et al.*, *Phys. Rev. Lett.* **21**, 1279 (1968).
- [15] S. Rock *et al.*, *Phys. Rev. Lett.* **24**, 748 (1970).
- [16] A. Airapetian *et al.*, *Phys. Lett. B* **682**, 351 (2010).
- [17] M. Alekseev *et al.* (COMPASS Collaboration), *Phys. Lett. B* **673**, 127 (2009).
- [18] A. Airapetian *et al.* (HERMES Collaboration), *Phys. Rev. Lett.* **103**, 152002 (2009).
- [19] E. Babcock, I. Nelson, S. Kadlecik, B. Driehuys, L. Anderson, F. Hersman, and T. Walker, *Phys. Rev. Lett.* **91**, 123003 (2003).
- [20] M. V. Romalis and G. D. Cates, *Phys. Rev. A* **58**, 3004 (1998).
- [21] M. Mihovilovic, K. Allada, B. Anderson, J. Annand, T. Averett *et al.*, *Nucl. Instrum. Methods Phys. Res., Sect. A* **686**, 20 (2012).
- [22] J. Alcorn *et al.*, *Nucl. Instrum. Methods Phys. Res., Sect. A* **522**, 294 (2004).
- [23] See Supplemental Material at <http://link.aps.org/supplemental/10.1103/PhysRevLett.113.022502> for details of background corrections.
- [24] S. Scopetta, *Phys. Rev. D* **75**, 054005 (2007).
- [25] X. Zheng *et al.*, *Phys. Rev. C* **70**, 065207 (2004).